ASEG-PESA 2015
Geophysics and Geology together for Discovery
24th International Geophysical Conference and Exhibition
15–18 February 2015 Perth, Western Australia

3D IP Inversion of Airborne EM data at Tli Kwi Cho

Seogi Kang*
University of British Columbia
Vancouver, BC V6T 1Z4 Canada
skang@eos.ub.ca

Douglas W. Oldenburg
University of British Columbia
Vancouver, BC V6T 1Z4 Canada
doug@eos.ubc.ca

Michael S. McMillan
University of British Columbia
Vancouver, BC V6T 1Z4 Canada
mmcmilla@eos.ubc.ca

SUMMARY

In this study, we revisit three airborne EM surveys over Tli Kwi Cho (TKC). These consist of a frequency domain DIGHEM data set, and two time domain surveys, VTEM and AeroTEM. Negative transients have been recorded in both of the time domain surveys and we interpret these as arising from chargeable bodies. The kimberlite pipes are referred to as DO-27 and DO-18. We look in more detail at the transient data and apply the ATEM-IP inversion procedure to recover a 3D pseudo-chargeability distribution. Important components of the analysis involve estimating a background conductivity for the region. For DO-27 we have used a 3D parametric inversion to recover the conductivity from TEM data. The IP signal for the inversion is obtained by subtracting the time domain responses estimated by EM inversion from the observed background signal. This process also removes EM coupling noise that might be contaminating the data. The resultant IP data are inverted with a linear inverse approach using the sensitivity from the background conductivity. This yields a 3D model of pseudo-chargeability.

INTRODUCTION

The Tli Kwi Cho (TKC) kimberlite complex, located 360 km north-east of Yellowknife, Northwest Territories, Canada, consists of two separate kimberlite pipes named DO-18 and DO-27. These were first identified in late 1992 from frequency domain airborne electromagnetic (EM) survey using the DIGHEM system (Figure 1). Since then two airborne time domain EM (ATEM) surveys have also been carried out using AeroTEM and VTEM systems. An important feature of the ATEM data is the existence of negative transients. The data collected in the AeroTEM and VTEM surveys show the existence of negative transients indicative of chargeable material (Weidelt, 1982; Smith and Klein, 1996). Jansen and Witherly (2004) have previously analysed these data and estimated Cole-Cole parameters for both kimberlite pipes.

Here we revisit these data but use new tools in 3D forward modeling (Marchant et al., 2012) and inversion (McMillan et al., 2014; Yang et al., 2014). We first present the data from the two different EM systems and show the negative transients. Second, we apply EM inversions separately to three different data sets and recover the conductivity. The 3D distributed IP information from the VTEM data is estimated by applying the linearized inversion method of Kang et al. (2014) . This result can be compared with other physical property models and geology.

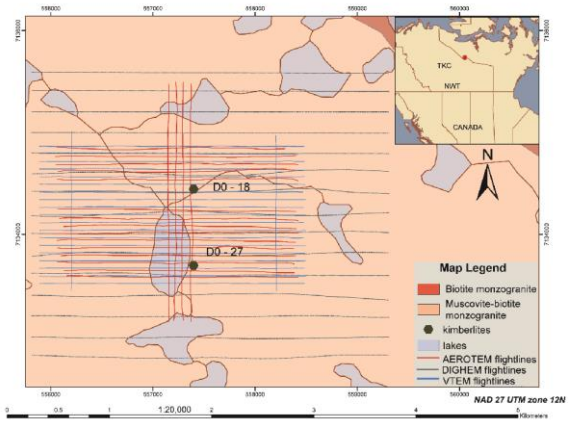

Figure 1: Geological map of the Tli Kwi Cho Kimberlite Complex in Northwest territories, Canada. Three surveys of DIGHEM, VTEM and AeroTEM in grey, blue and red, respectively.

EM SYSTEMS AND DATA

The specifications for the both frequency and time domain EM systems are provided in Table 1. The first is the DIGHEM system. This frequency domain system has five frequencies ranging from 900-56k Hz and two distinct Tx-Rx geometries, which are horizontal coplanar (HCP) and vertical coaxial (VCA); Tx-Rx separations of all loops are 8 m except for 56k Hz loops (6.3 m). The 900 Hz anomaly map is shown in Figure 2 and it delineates two anomalies named DO-18 and DO-27. Two time domain systems, AeroTEM and VTEM were also flown.

Specs	DIGHEM	VTEM	AeroTEM
Type	Frequency	Time	Time
Waveform	sinusoidal	trapezoidal	triangular
t or f range	900-56k Hz	90-6340 μs	26-1393 μs
t or f channels	5	27 off-time	16 off-time
Geometry	HCP, VCA	HCP	HCP
Offset	8 or 5 m	0 m	0 m
Tx-Rx height	~30 m	~28 m	~28 m
Year of flight	1992	2004	2003
Data type	B_z or B_x	$\frac{dB_z}{dt}$	$\frac{dB_z}{dt}$, $\frac{dB_x}{dt}$
Data Unit	ppm	$pV/A\text{-}m^4$	nT/s

Table 1: Specifications of three different airborne EM systems.

Both ATEM systems use a HCP Tx-Rx geometry in a coincident loop configuration and data measured in the off-time. A principal difference between the two systems is the

waveform; VTEM uses a trapezoidal waveform with an on-time pulse of 4.5 ms and a base frequency 30 Hz and AeroTEM uses a triangular waveform with an on-time pulse of 1.10 ms and a base frequency of 150 Hz.

In Figure 2a, we present the quadrature component EM responses at 900 Hz from the DIGHEM survey. These data can be converted to apparent conductivity and the overall background conductivity was ~1000 ohm-m, which is quite resistive and is reasonable value for granitic host. Measured EM responses from three different systems show two distinctive anomalies: DO-27 and DO-18. A region near DO-27 in quadrature component of DIGHEM data (Figure 2a) has high anomaly, which possibly indicates a conductive feature. Similarly, we observe high anomaly near this region on the shaded maps of AeroTEM responses at t=52 µs (Figure 2b) and VTEM responses at t=220 µs (Figure 3a). Negative transients are observed near this region in VTEM responses at t=410 µs as shown in Figure 3b.

Conversely, DIGHEM responses for DO-18 also show a high anomaly, which similarly may indicate a conductive feature. Different from DO-27, consistent negative transients are observed near DO-18 in both time domain EM systems. Those features can be clearly recognized in the South-North profile of AeroTEM data (Figure 4b). Even though we observe negative transients in both DO-27 and DO-18, they have different time decaying features. At both t=220 and 410 µs, VTEM responses near DO-18 show consistent negatives (Figure 3a and b). In contrast, as shown in the East-West profile of VTEM (Figure 4a), responses near DO-27 show a high anomaly at early time channels (150-350 µs), and negative transients start to emerge only at 410 µs.

In summary, the EM data indicate two regions of higher conductivity, both of which have a chargeable response. Away from the two conductors the responses are small and reflect a resistive background as shown in Figure 4. Negative transients near DO-27 and DO-18 showed different time decaying patterns. Consistent negative transients near DO-18 even at the earliest time channel of VTEM data, are challenges for EM inversion, since those negatives cannot be explained EM forward modelling without including IP effects.

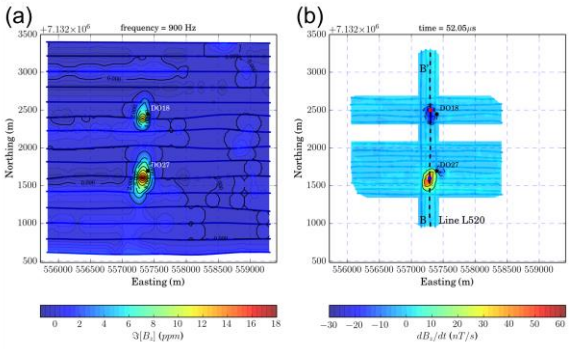

Figure 2: Interpolated map for DIGHEM and AeroTEM data. (a) The quadrature component of B_z at 900 Hz obtained from the DIGHEM system (HCP Tx). (b) dB_z/dt responses at obtained 52 µs from AeroTEM.

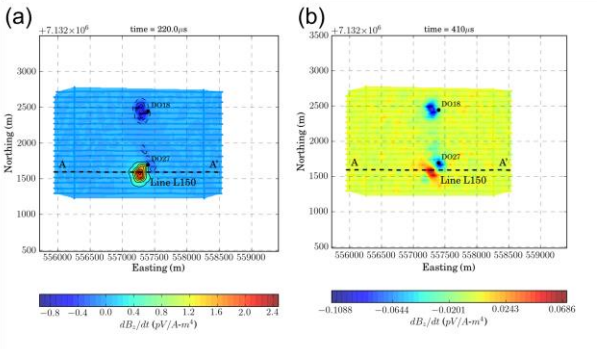

Figure 3: Interpolated map VTEM responses. (a) dB_z/dt at t = 220 µs. (b) dB_z/dt at t = 410 µs. Black dotted lines show the location of L150, which crosses the center of DO-27 anomaly from east to west.

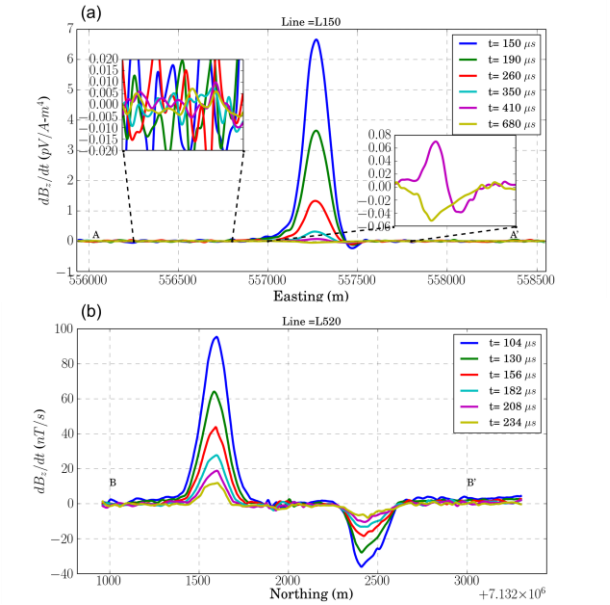

Figure 4: Profiles of VTEM and AeroTEM responses. (a) VTEM profiles along line, L150. (b) AeroTEM profiles along line, L520. The lines L150 for VTEM and L520 AeroTEM are marked as black dashed lines on Figures 3 and 2b, respectively.

3D CONDUCTIVITY INVERSION

We can perform 3D ATEM conductivity inversion by omitting IP contaminated data and carrying out an inversion. Thus a strategy of using only early time data for VTEM survey over DO-27 can work. For the inversion we extract stations near DO-27 and filtered all negative transients in the data. The kimberlite is a compact conductive object in a resistive background and hence we used a 3D parametric inversion algorithm (McMillan et al., 2014) to invert the data. In this approach, distributed model parameters were parameterized as a skewed Gaussian ellipsoid model, which is a single body model in the earth. Nine parameters were used to describe geometry of that body and two parameters were used for conductivity values of the inside and outside of the body. The recovered conductivity model is shown in Figure 5 and there is a reasonable match with geological model (Figure 5b). The inversions of the other EM data sets, as well as the VTEM data over DO-18, are still in progress.

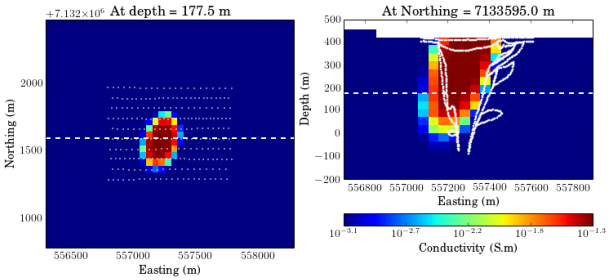

Figure 5: 3D conductivity from parametric inversion of the ATEM. Right and left panels show plan and section views of 3D model. Plan and section views slice the depth at 177.5 m and the northing 7133645 m (white dashed lines). White lines on right panel outlines geological boundaries.

ATEM-IP INVERSION PROCEDURE

To carry out the IP inversion we apply the processing and linear inversion procedure suggested by Kang et al. (2014). We concentrate upon VTEM data over DO-27. There, the IP responses are embedded in the measured data at early time channels and then emerge at later time channels.

Following the notation used in Smith et al. (1988) any EM field, d can be expressed as the summation of d^{IP} and d^{F}, where d denotes the measured response, d^{IP} is standalone IP field and d^{F} is EM field without IP effects. We define the IP datum, d^{IP}, as

$$d^{IP} = d - d^{F} \quad . \tag{1}$$

Since this subtraction process removes EM coupling, IP responses in various time ranges can be better identified. To obtain the fundamental EM response, d^{F}, we first recover a 3D conductivity model as in the previous section. Forward modelling then yields an approximate value of d^{F}. However, we cannot get the correct d^{F}, since the estimated background conductivity is not exact. Therefore the computed d^{IP} data may contain a residual field due to the incorrect background conductivity. We assume this residual field is a large-scale smoothly varying perturbation to the d^{IP} data and refer to it as regional field. To estimate it, we fit the computed d^{IP} data with a low order polynomial and subtract that from the d^{IP} data. In addition, since d^{IP} data should be negative in late time channels, we replace all positive values in the regionally corrected d^{IP} data with zeros. We refer to this process as positive thresholding. This regional removal process can be expressed as

$$d^{IP} = d^{obs} - d[\sigma_{est}] - \delta d = raw\ d^{IP} - \delta d \quad , \tag{2}$$

where σ_{est} is the background conductivity model estimated from 3D ATEM inversion, $d[\sigma_{est}]$ is the forward modelled data from σ_{est}, and δd arises from the regional processing. Here we let $raw\ d^{IP} = d^{obs} - d[\sigma_{est}]$. The sequence of data processing is illustrated in Figure 6 which shows the VTEM data at t=410 µs. The observed data are shown in Figure 6a and the forward modelled EM data in Figure 6b ($d[\sigma_{est}]$). Subtraction yields the $raw\ d^{IP}$ data, (Figure 6c) and the regional-removed d^{IP} data with positive thresholding are shown in Figures 6d. The importance of subtracting the EM response ($d[\sigma_{est}]$) from the observations (d^{obs}) is clearly shown.

3D IP INVERSION

Since d^{IP} data are linearly related to the pseudo-chargeability we can write

$$d_i^{IP} = \mathbf{J}\tilde{\eta}_i, \tag{2}$$

where $\tilde{\eta}(t)$ is pseudo-chargeablity, **J** is the sensitivity matrix and subscript i indicates i^{th} time channel. The choice of what sensitivity is used for the airborne system is outlined in Kang et al. (2014). Based on this forward relationship, the linearized inversion can be applied separately for each time channel to recover the 3D distribution of pseudo-chargeability for each time channel.

The linearized inversion is applied to the corrected d^{IP} data in Figure 6d to recover a 3D distribution of pseudo-chargeability. We present plan and sectional views of the pseudo-chargeability in Figure 7. The white line in this figure outlines geological boundaries based on drilling results (Harder et al., 2008). The recovered IP body at the center seems to shows similar geometric features with the conductivity model on plan view (Figure 7a). In section view (Figure 7b), the anomalous IP body is located near the interface between the background rock and kimberlite pipe. This might be geologically reasonable if the interface was a conduit for the fluids that caused alteration products that were chargeable. The linearized inversion also revealed another IP body, which has smaller magnitude of pseudo-chargeability (left panel of Figure 7). This feature is required by the data but its existence requires further scrutiny. In Figure 8 we present 3D volumes of recovered conductivity and pseudo-chargeability models overlaid with the outline of the kimberlite from geologic drilling.

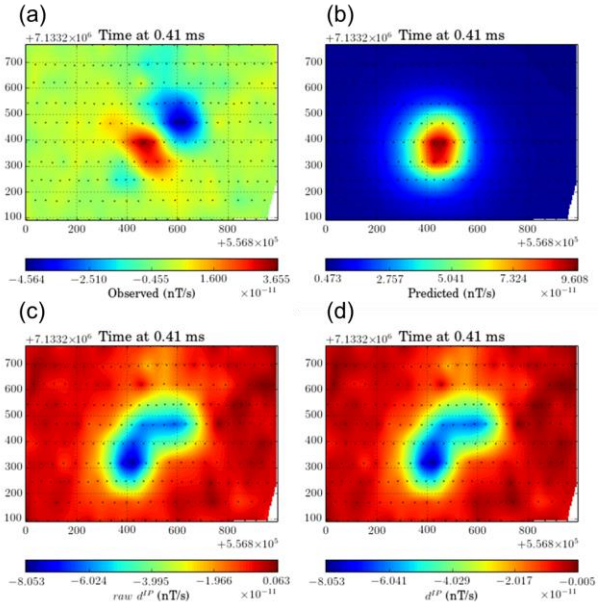

Figure 6: Processing of d^{IP} data: (a) d^{obs}, (b) $d[\sigma_{est}]$, (c) $raw\ d^{IP}$ and (d) d^{IP} responses. Black dots show the locations of stations.

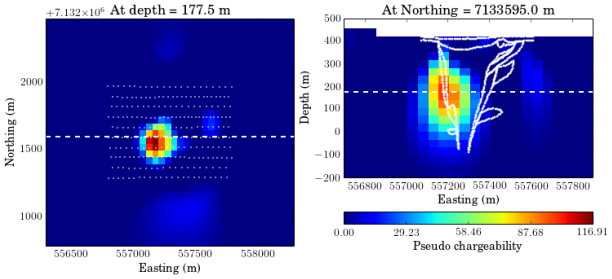

Figure 7: 3D pseudo-chargeability model from the linearized inversion of d^{IP} data at t=410 µs. A plan view is plotted in the left panel and cross section is plotted on the right. White dots in the left panel show the station locations used in the linearized inversion of d^{IP} data.

CONCLUSIONS

Multiple airborne EM data sets obtained at the TKC kimberlite complex are revisited with modern technologies including 3D EM forward modeling and inversion to recover 3D IP information. The emphasis thus far has been on using VTEM data over DO-27 to recover a 3D conductivity and pseudo-chargeability. A 3D parametric inversion was used to estimate a compact conductivity model. The computed d^{IP} data, obtained by subtracting predicted EM data from the observed data, is an important step in the process. It allowed us to recognize IP signal that was buried in the measured ATEM data. By inverting the d^{IP} data with the linearized inversion approach, we recovered a 3D distribution of the pseudo-chargeability. The recovered IP body is shifted somewhat from the main conductivity and is located along boundary between the kimberlite pipe and the host rock. This might be geologically reasonable if the contact was a conduit for fluids causing alteration products.

The TKC data sets have been valuable in helping us develop our forward modelling and inversion strategies for IP data and it has opened up new areas for research. In particular we have yet to contend with inverting VTEM data over DO-18 where the data are negative even at the earliest time channels. Also, there is the ultimate challenge of finding a single conductivity and a single chargeability model that is compatible with all three EM data sets.

ACKNOWLEDGMENTS

We thank Ken Witherly and Condor Consulting, Inc. for providing data and background information about TKC. We would like to thank Dom Fournier and other UBC-GIF members for their participation in processing EM data sets and investigating the geological background of this region.

REFERENCES

Harder, M., Hetman, C. M., Scott Smith, B. H. and Pell J., 2008, The evolution of geological models for DO-27 kimberlite, NWT, Canada: implications for evaluation: 9th meeting IKC, Frankfurt, Expanded Abstracts, 1-3.

Jansen, J., and Witherly, K., 2004, The tli kwi cho kimberlite complex, northwest territories, canada: A geophysical case study: 74th meeting SEG, Denver, Expanded Abstracts, 1147–1150.

Kang, S., Oldenburg D. W., D. Yang, and D. Marchant, 2014, On recovering induced polarization information from airborne time domain EM data: 84th meeting SEG, Denver, Expanded Abstracts, 1785–1789.

Marchant, D., Haber, E., Beran, L., and Oldenburg, D. W., 2012, 3D modeling of IP effects on electromagnetic data in the time : 82th meeting SEG, Las Vegas, Expanded Abstracts, 1-5.

Michael, S. M., Schwarzbach, C., Oldenburg, D. W., Haber E., Holtham E., and Prikhodko, A., 2014, Recovering a thin dipping conductor with 3D electromagnetic inversion over the Caber deposit: 84th meeting SEG, Denver, Expanded Abstracts, 1720-1724

Smith, R., and Klein, J., 1996, A special circumstance of airborne inducedpolarization measurements: Geophysics, 61, 66–73.

Smith, R., Walker, P., Polzer, B., and West, G. F., 1988, The time-domain electromagnetic response of polarizable bodies: an approximate convolution algorithm: Geophysical Prospecting, 36, 772–785.

Weidelt, P., 1982, Response characteristics of coincident loop transient electromagnetic systems: Geophysics, 47, 1325–1330.

Yang, D., Oldenburg, D. W., and Haber, E., 2014, 3-d inversion of airborne electromagnetic data parallelized and accelerated by local mesh and adaptive soundings: Geophysical Journal International, 196, 1942–1507.

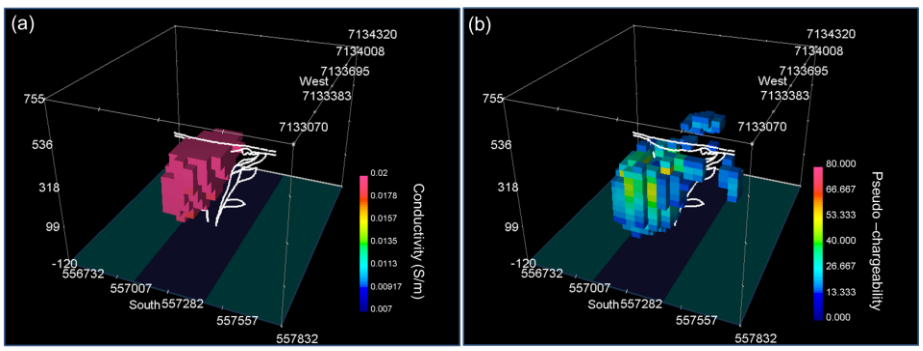

Figure 8: 3D volume rendered images: (a) conductivity model and (b) pseudo-chargeability model.